Heliyon 9 (2023) e21202

Contents lists available at ScienceDirect

Heliyon

journal homepage: www.cell.com/heliyon

# Evaluating the hepatotoxic versus the nephrotoxic role of iron oxide nanoparticles: One step forward into the dose-dependent oxidative effects

Basma Emad Aboulhoda [a,*], Doaa Abdullah Othman [a], Laila A. Rashed [b], Mansour A. Alghamdi [c,d], Abd EL Wakeel E. Esawy [a]

[a] Department of Anatomy and Embryology, Faculty of Medicine, Cairo University, Egypt
[b] Department of Biochemistry and molecular biology, Faculty of Medicine, Cairo University, Egypt
[c] Department of Anatomy, College of Medicine, King Khalid University, Abha, 62529, Saudi Arabia
[d] Genomics and Personalized Medicine Unit, College of Medicine, King Khalid University, Abha, 62529, Saudi Arabia

ARTICLE INFO

*Keywords:*
*Iron nanoparticles*
Kidney
Liver
Immunohistochemistry
Oxidative stress

ABSTRACT

The present study has been designed to detect the dose-dependent effect of iron oxide nanoparticles (IONPs) on the liver and kidney of rats by evaluating three different doses 30, 300, 1000 mg/kg/day IONPs for 28 days. Forty rats were divided into four groups; I (control), II (low dose), III (medium dose) and IV (high dose).

There also was a statistically-significant elevation in the serum levels of hepatic enzymes; AST and ALT in medium & high dose. The elevation of serum ALP, on the other hand, was significant in all IONPs doses.

There was significant elevation in the levels of urea creatinine, and MDA in the medium and high doses of IONPs. The activity of superoxide dismutase (SOD) and glutathione peroxidase (GPx) showed significant decrease in the high dose only compared to the control group.

The serum iron levels increased in a dose-dependent manner in the IONPs-treated groups with highly significant increase in the moderate and high dose groups.

On comparing the effect of different doses of IONPs between the liver and kidney, the high dose revealed statistically significant difference ($p < 0.05$) in the area percent of collagen deposition ($54.4 \pm 3.9$ versus $6.1 \pm 2.6$) and alpha smooth muscle actin (α-SMA) reaction ($7.7 \pm 1.5$ versus $17.8 \pm 4.3$) in the liver relative to the kidney. The medium and high doses revealed statistically significant difference in optical density of Periodic acid Schiff (PAS) reaction ($45 \pm 3.4$ versus $50.3 \pm 1.8$ in the medium dose, and $38.9 \pm 6$ versus $63 \pm 3$ in the high dose) and area percent of inducible nitric oxide synthase (iNOS) reaction ($12.98 \pm 2.7$ versus $3.5 \pm 0.5$ in the medium dose, and $27.91 \pm 1.5$ versus $7.7 \pm 0.6$ in the high dose) in the liver relative to the kidney.

## 1. Introduction

The widespread use of Iron oxide nanoparticles (IONPs) in several biomedical, agricultural and environmental fields has urged the scientific community to investigate their potential toxicity for the purpose of developing novel strategies for human safety [1].

* Corresponding author. Department of Anatomy and Embryology Faculty of medicine-Cairo University, Egypt.
*E-mail address:* basma.emad@kasralainy.edu.eg (B.E. Aboulhoda).

https://doi.org/10.1016/j.heliyon.2023.e21202
Received 6 July 2023; Received in revised form 13 September 2023; Accepted 18 October 2023
Available online 24 October 2023

Despite the involvement of IONPs in numerous industries and water purification systems, yet, the most crucial application of IONPs is in the field of biomedicine especially in magnetic resonance imaging, tumor localization, gene therapy and tissue healing [2]. These medical applications necessitate direct introduction of IONPs into the human body with increasing concerns about the possible toxic consequences [3]. Thus, the current study has been designed to elucidate the effect of IONPs, on the liver and kidneys as the most crucial organs involved in metabolism and excretion of drugs and toxins.

Since the concentration of nanoparticles is the most critical factor governing their toxicity [4], the present study has evaluated the effect of three doses of IONPs (30, 300 and 1000 mg/kg/day).

To shed light on the mechanisms underpinning the potential hepatorenal toxicity of IONPs, the study has evaluated the effect of these nanoparticles on the antioxidants and free radical scavenging system of the liver and kidneys via demonstrating the dose dependent effect on the malondialdehyde (MDA), Glutathione peroxidase (GPx) and superoxide dismutase (SOD) activity.

## 2. Material and methods

### 2.1. Chemicals

Iron oxide NPs (98 %) ($Fe_2O_3$-30 nm) were purchased from Sigma-Aldrich Company in Egypt in the form of a powder of 100 g dissolved in 100 ml saline solution. Iron oxide nanoparticles characterization was done using transmission electron microscopy (TEM ((JEOL JEM 1010, Japan).

### 2.2. Animals

*Sprague-Dawley* male albino rats (150–200 g) were included in the study. The rats were provided by the Animal House, Kasr Alainy, Faculty of Medicine, Cairo University. The rats were bred under standard laboratory and environmental conditions with free access to standard rodent pellets and water *ad libitum*. The study was approved by Kasr Alainy Ethics Committee and the Institutional Animal Care and Use Committee (IACUC) (approval number CU-III F14-19). The study had been conducted according to the ethical standards of the National Institutes of Health guide for the care and use of Laboratory Animals (NIH Publications No. 8023, revised 1978).

### 2.3. Experimental design

To understand the dose-toxicity relationship, the animals were randomly-allocated into 4 groups, ten rats each; group I (control) received no medication, group II (low dose): received 30 mg/kg/day IONPs, group III (medium dose): received 300 mg/kg/day IONPs, group IV (high dose): received 1000 mg/kg/day IONPs. IONPs were administered once daily for 28 days using gastric gavage [5].

No mortality was recorded. At the end of the experiment, the rats were anaesthetized using via intra-peritoneal injection of phenobarbital sodium (40 mg/kg). Blood samples were collected from the retro-orbital plexus of veins for assessment of hepatic and renal functions. The rats were then euthanized by cervical dislocation and the liver and kidneys were dissected. Part of the specimens was taken for biochemical study to measure the oxidative markers; the other part was fixed in 10 % buffered formol saline and prepared for paraffin blocks.

The sections were subjected to.

1. Light microscopic examination

The liver and kidney tissues were cut to 5 μm sections and stained with Haematoxylin and eosin (H&E) staining for routine histological study, masson's trichrome (MT) staining for detection of collagen, and Periodic acid Schiff reaction (PAS) to study the density of glycogen granules.

2. Immunohistochemistry for inducible nitric oxide synthase (iNOS) and α-smooth muscle actin (α-SMA):

Immunohistochemical staining for anti iNOS antibodies and anti α-SMA was conducted by streptoavidin–biotin method [6]. The sections were incubated with the primary antibodies; rabbit polyclonal anti-α-SMA (ab5694), at a 1:100 dilution, IHC-P, species specificity including rats, Abcam) and inducible nitric oxide synthase (iNOS) (ab3523, 1:100) (Abcam, Cambridge, MA, USA) antibodies. The specimens were counterstained with H&E.

2. Biochemical assay

Serum samples were used for evaluation of alanine aminotransferase (ALT) aspartate aminotransferase (AST), alkaline phosphatase (ALP) along with the serum urea, creatinine and iron level by conventional colorimetric method according to the manufacturer's instructions (BioMed-GPT, BioMed diagnostics, Egypt).

## 3. Measurement of oxidative/antioxidative markers

Superoxide dismutase (SOD) and Glutathione peroxidase (GPx) activities in the liver and kidney tissue homogenates were

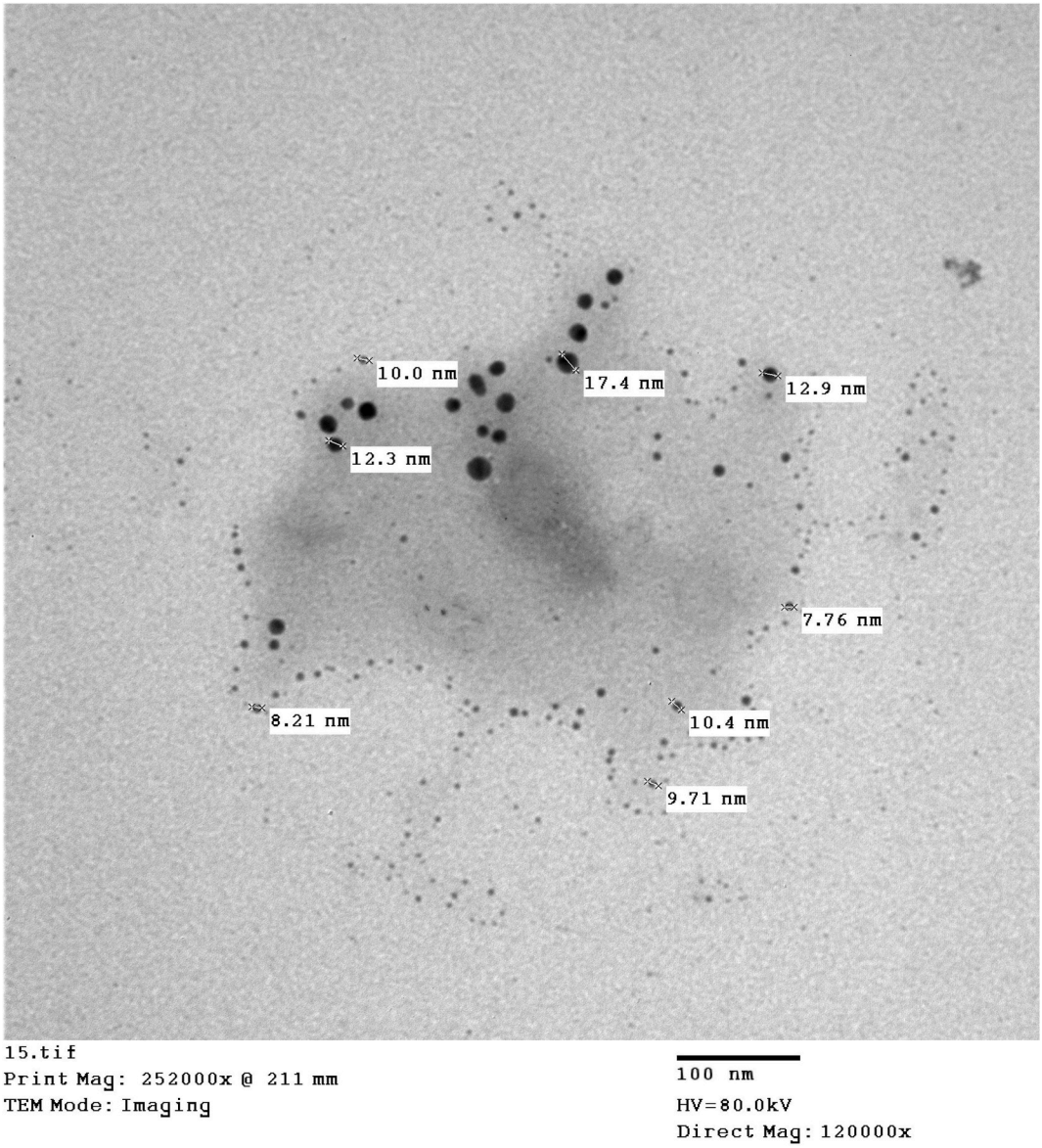


**Fig. 1.** An electron micrograph displaying TEM imaging of spherical iron oxide nanoparticles (IONPs) showing the particle size at nanoscale ranging from 7.76 nm to 17.4 nm (**TEM x120000,** scale bar 20 nm).

measured by the inhibition of nitroblue tetrazolium reduction by $O_2$-generated by the xanthine/xanthine oxidase system. The level of malondialdhayde (MDA) as an index of the extent of lipid peroxidation in the tissues was also estimated (MyBiosource, Science and Technology, Egypt).

### *3.1. Morphometric measurements*

A quantitative histomorphometric study was performed using the image J analysis system (Image Pro Plus 6.0, Media Cybernetics, USA) and the Lica Qwin 500 LTD software (England). The study involved assessment of the area percent of collagen in Masson's trichrome sections, the mean optical density of PAS reaction and the area percent of iNOS and αSMA immune-reactivity in ten non-overlapping microscopic fields under magnification 400 [7].

### *3.2. Statistical analysis*

Data were analyzed via SPSS software using one-way analysis of variance (ANOVA) and Bonferroni post hoc testing. The data were summarized as mean ± standard deviation. P-values $<0.05$ were regarded statistically-significant.

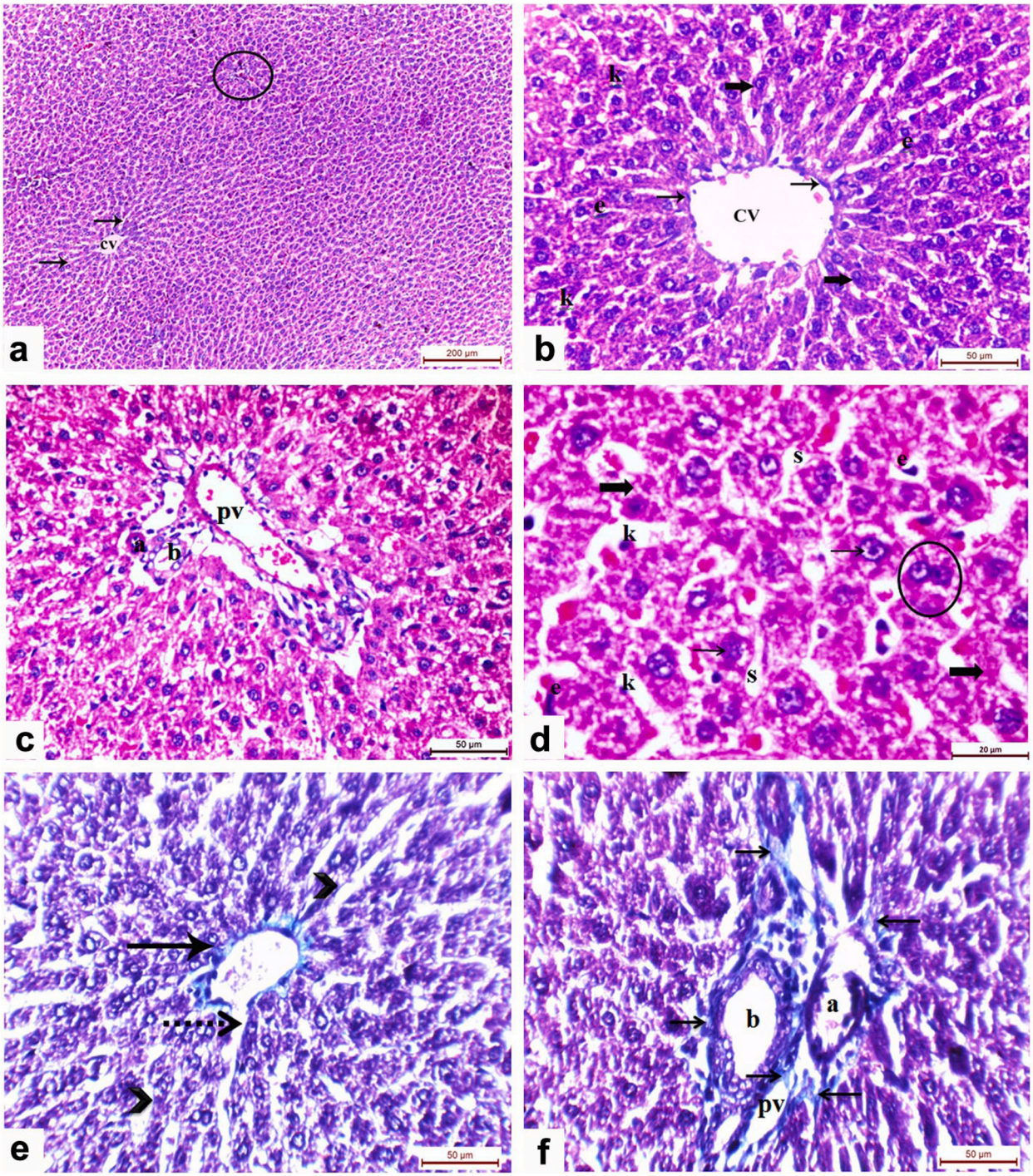


**Fig. 2.** Photomicrographs of rat liver sections from group I (control) showing (a) showing the classic hepatic architecture with hepatocytes arranged in cords radiating from the central vein (cv) with narrow sinusoids in-between (arrows). The portal area is seen at the periphery of the hepatic lobule (circle). (b) Higher magnification demonstrates the central vein (cv) lined with flat endothelial cells (thin arrows). The hepatocytes are polyhedral (thick arrows) in shape. The plates of hepatocytes are separated by blood sinusoids lined by endothelial cells (e) and von Kupffer cells (k). (c) The portal area display the portal vein (pv), branch of the hepatic artery (a) and bile duct (b). (d) Higher magnification demonstrates hepatocytes with acidophilic cytoplasm (thick arrows) and central vesicular basophilic nuclei (thin arrows) separated by narrow blood sinusoids (s) lined by endothelial (e) and von Kupffer cells (k). The hepatocytes show occasional binucleation (circle). (e–f) Masson trichrome stain demonstrates (e) thin collagen fibers distributed around the central vein (arrow) and the hepatic sinusoids (arrow heads). The collagen was also seen radiating for a short distance along the wall of the blood sinusoids (doted arrow). (f) The portal area demonstrates normal thin collagen fibers (arrows) around the portal vein (pv), the hepatic artery (a) and the bile duct (b).

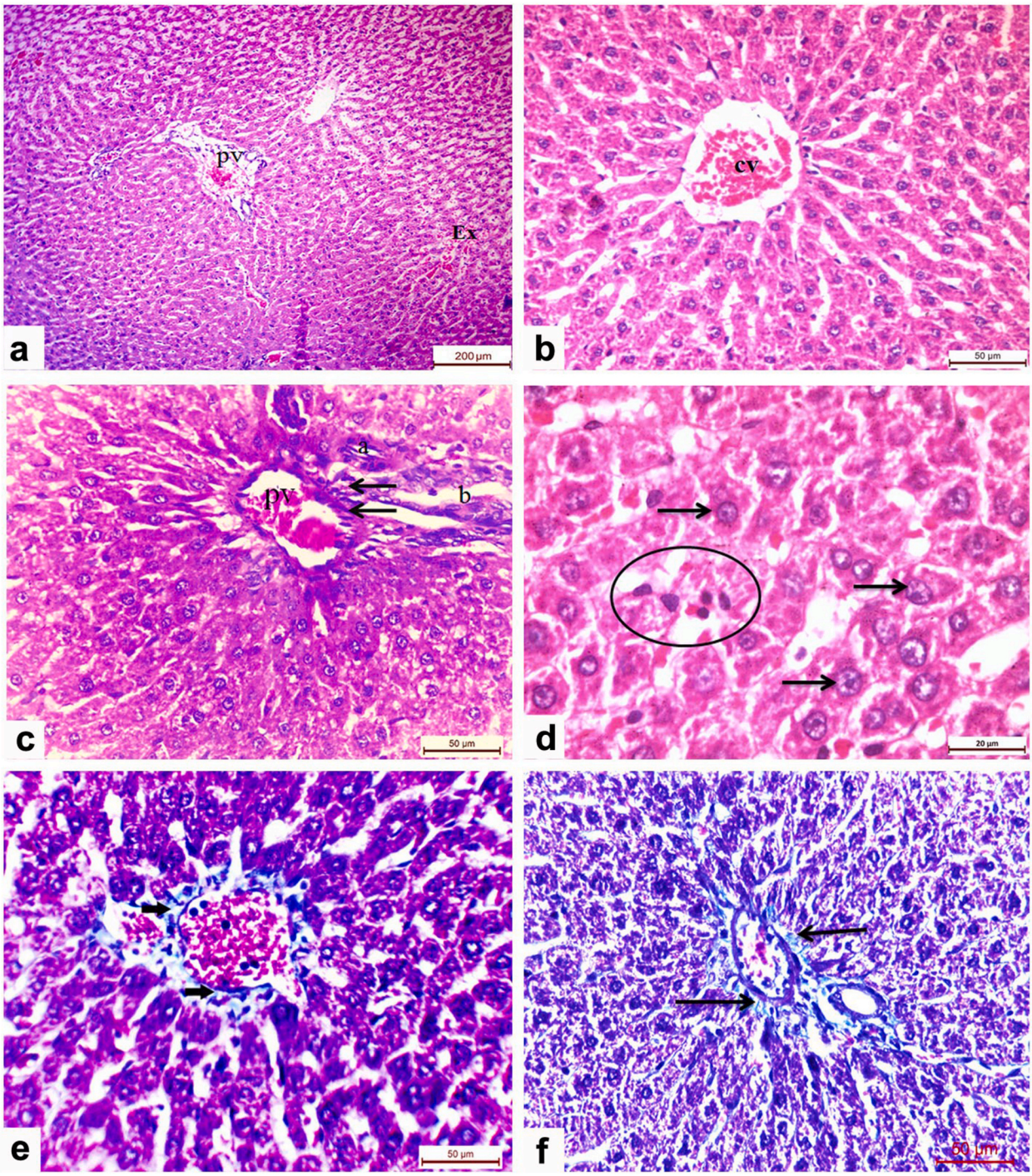


**Fig. 3.** A photomicrograph of a section in rat liver from group II (low dose) showing (a) disturbed architecture of the portal vein (pv) which appears mildly-dilated and congested. Blood extravasation (Ex) is also noticed. (b) The central vein (cv) also appears mildly congested. (c) Inflammatory infiltrate (arrows) is also seen in the vicinity of mildly-dilated and congested portal vein (pv), hepatic arteriole (a) and bile ductule (b). (d) Focal proliferation of von Kupffer cells (circle) are seen in between the hepatocytes (arrows). (e–f) Masson trichrome stain demonstrates minimal increase of collagen deposition (arrows) around the central vein (e), and around the portal area (f).

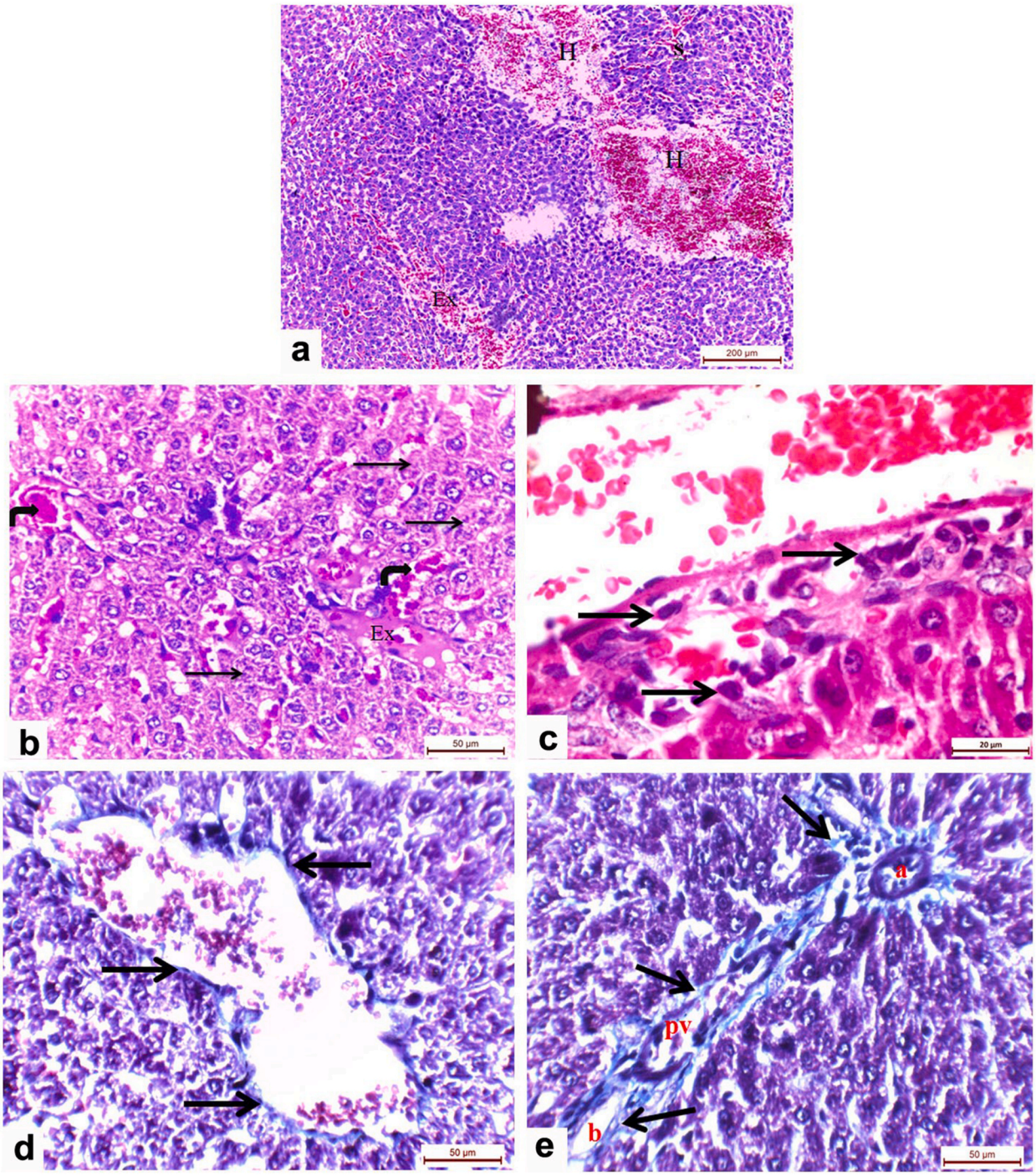


**Fig. 4.** A photomicrograph of a section in rat liver from group III (medium dose) showing (a) massive areas of interstitial hemorrhage (H), dilated congested blood sinusoids (s) and vast areas of blood extravasation (Ex). (b) High magnification shows marked distortion of the liver architecture, acidophilic masses (curved arrows) and areas of exudation (Ex). Degenerated hepatocytes with disintegrated cytoplasm (arrows) can also be observed. (c) Perivascular inflammatory cellular infiltration (arrows). (d–e) Masson trichrome stain demonstrates minimal increased amount of collagen deposition (arrows) around the central vein (d) and in the portal area around the hepatic artery (a), the portal vein (pv) and the bile duct (e).

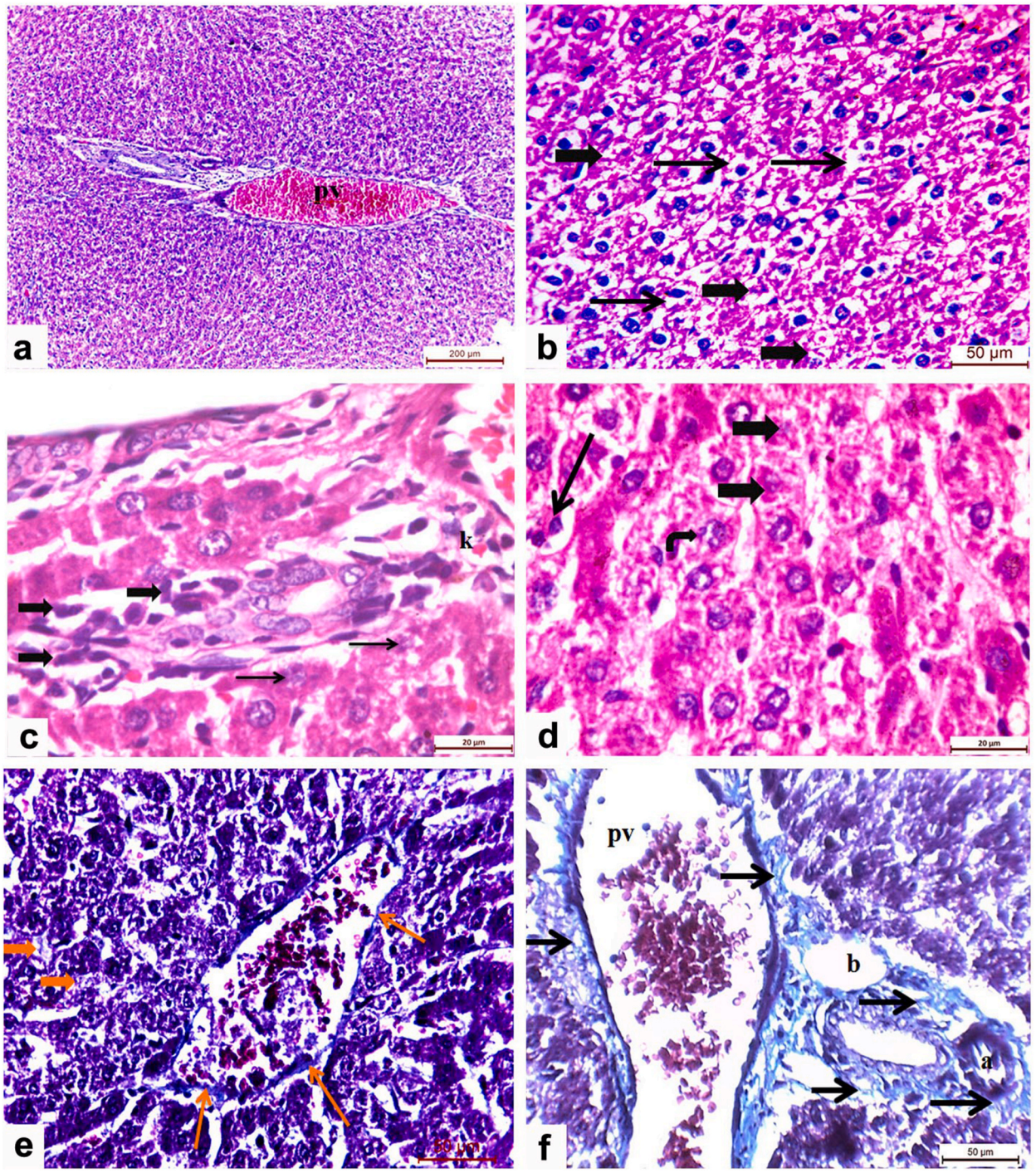


**Fig. 5.** A photomicrograph of a section in rat liver from group IV (high dose) group showing (a) marked dilatation and congestion of portal vein (pv). (b) High magnification shows degenerated hepatocytes with marked cytoplasmic vacuolations (thin arrows). Some nuclei show karyorrhexis (thick arrow). (c) Proliferation of von kupper cells (k) and periportal inflammatory cellular infiltration (thick arrows). Nuclear changes in the form of ghost nuclei (thin arrows) can be observed. (d) Several nuclear changes such as pyknosis (thin arrow), karyorrhexis (curved arrow) and karyolysis (thick arrows) are also observed. (e–f) Masson trichrome stain demonstrates massive increase in deposition of collagen bundles around the central vein (thin arrow). Augmented amount of interstitial collagen is also observed (thick arrow).and in the portal area around the hepatic artery (a), the portal vein (pv) and the bile duct (b).

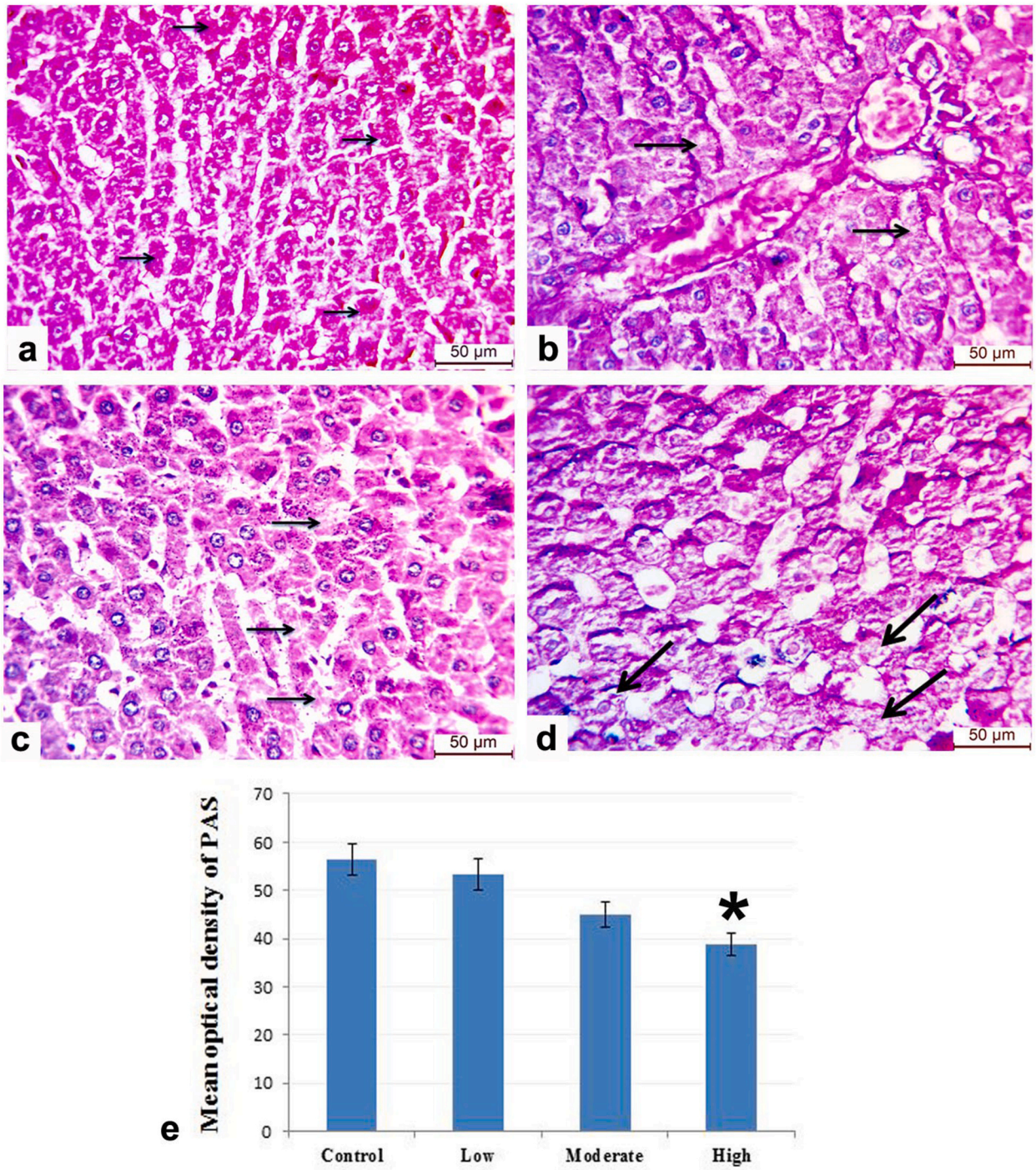


**Fig. 6.** (a) group I (control) showing strongly positive PAS magenta red glycogen granules in the cytoplasm of the hepatocytes (arrows), (b) Low dose IONPs group displays variable degrees of glycogen depletion among hepatocytes (arrows). (c) Medium dose IONPs group demonstrates obvious reduction of glycogen content in the majority of hepatocytes (arrows) (d) High dose IONPs group demonstrates marked reduction in the PAS-positive granules in most of the hepatocytes (arrows). (e) Optical Density of PAS in the different study groups ($n = 6$); data are presented as mean ± SD. *: Statistically significant compared to control group at $P < 0.05$ using ANOVA, Bonferroni post-hoc pairwise comparison, (PAS: Periodic acid Schiff) (scale bar 50 μm). (For interpretation of the references to color in this figure legend, the reader is referred to the Web version of this article.)

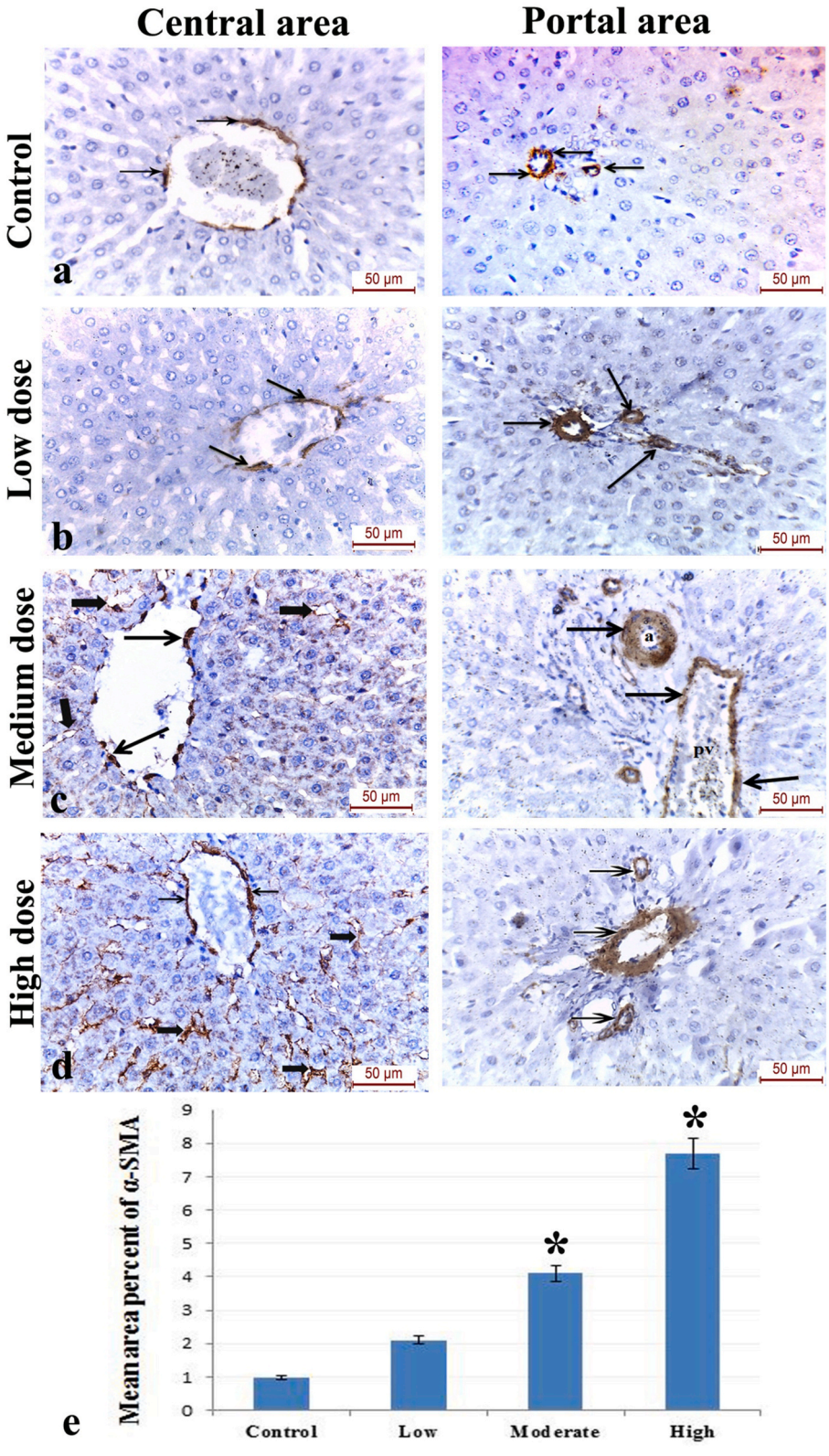


*(caption on next page)*

**Fig. 7.** A photomicrograph of a section in the rat liver from (a) group I (control) showing (a) single layer of α-SMA positive cells around the central vein (arrows) and weak α-SMA positive cells around the portal vessels (arrows). (b) group II (Low dose) shows mild immunereactivity around the central vein (arrows) and increased α-SMA immunereactivity the media of the vessels of the portal area (c) group III (Medium dose) shows strong positive α-SMA immunoreaction in the wall of the central vein (thin arrows) and the blood sinusoids (thick arrows) and in the media of a dilated portal vein (pv) and a thickened hepatic artery (a). (d) group IV (High dose) shows intense positive α-SMA immunoexpression around the central vein (thin arrows), in the blood sinusoids between the hepatocytes (thick arrows) and in the media of the portal area vessels. (e) Area percentage of α-SMA immunreactivity in the different study groups (n = 6); data are presented as mean ± SD. *: Statistically significant compared to corresponding value in the control group at $P < 0.05$ using ANOVA, Bonferroni post-hoc pairwise comparison, (scale bar 50 μm).

## 4. Results and discussion

### 4.1. Confirmation of particle size of IONPs

Transmission electron microscopy (TEM) revealed spherical, loosely agglomerated IONPs with a size of less than 17 nm in diameter (Fig. 1).

### 4.2. Effect of IONPs on the hepatic pathological changes

Examination of the H&E sections of the control group shows normal hepatic architecture with thin collagen fibrils around the central vein and portal area Fig. 2(a–f). The low dose group showed disturbed structure of the portal vein which appeared mildly-dilated and congested with occasional blood extravasation and inflammatory infiltrates. The central vein also appeared mildly congested. Focal proliferation of von Kupffer cells was observed in-between the hepatocytes Fig. 3(a–f).

The medium dose group showed massive areas of interstitial hemorrhage, dilated congested blood sinusoids and vast areas of blood extravasation Fig. 4(a–e). Those vascular changes could be attributed to the direct effect of IONPs on the vascular endothelial cells [5, 8].

Degenerated hepatocytes with disintegrated cytoplasm and perivascular inflammatory cellular infiltration were also observed.

The centri-lobular and peri-portal mononuclear cell infiltration in the liver parenchyma could be explained by the proinflammatory effect caused by accumulation of IONPs in tissues with subsequent increase in the macrophages [9].

In the high dose group, the congestion became more severe with subsequent blood extravasation and Von-Kupffer cell proliferation Fig. 5(a–f).

Kupffer cell proliferation represents a defense mechanism for engulfing the degenerated hepatocytes and the extravasated blood cells. The rate of metabolism in the Von-Kupffer cell depends upon the concentration of IONPs taken up by the cells [10]. A plethora of Kupffer cells was previously observed in mice treated with 150 and 300 μg/gr IONPs with histopathological changes comparable to our results [8].

Cytoplasmic vacuolation was another remarkable finding in high dose IONPs-treated rats. This cytoplasmic vacuolization could be a sequence of lipid peroxidation as a part of abnormal fatty degeneration or it could be a result of damaged or fragmented endoplasmic reticula [11].

The current study also elucidated areas of hepatic degeneration with disintegrated cytoplasm and several nuclear changes such as pyknosis, kaoryorrhexis, karyolysis and ghost nuclei in the IONP-treated groups. Degeneration is usually seen with toxicants affecting the nucleus, endoplasmic reticulum, mitochondria and cell membrane [12]. The resulting hepatocytes degeneration due to IONPs exposure may indicate an effect on protein synthesis by hepatocytes.

The IONPs' deleterious effect was not only observed in the hepatic parenchyma, but also in the hepatic stroma with increased collagen deposition around the portal area, central vein and in between the hepatocytes. This could be explained by irreversible liver damage that occurred with long duration of IONP administration in the current study (28 days).

### 4.3. Effect of IONPs on the hepatic glycogen storage

Assessment of PAS-stained sections of the control group displayed strongly-positive PAS magenta red glycogen granules in the cytoplasm of the hepatocytes (Fig. 6a). The low dose IONPs group displayed variable degrees of glycogen depletion (Fig. 6b). The medium dose group demonstrated obvious decline of glycogen content in the majority of hepatocytes (Fig. 6c). The high dose IONPs group revealed marked reduction in the PAS-positive granules in most of the hepatocytes (Fig. 6d) with statistically-significant reduction in the PAS optical density (Fig. 6e).

The remarkable depletion in the glycogen stores especially-observed in the moderate and high dose groups could be attributed to the hepatic damaging effect induced by INOPs which makes the hepatocytes incapable of storing glucose in the form of glycogen [13].

### 4.4. Immuno-histochemical evaluation of α-SMA in the liver tissue

The alpha-SMA is a crucial marker of fibrogenesis present in the microfilaments of the vascular smooth muscle cells and contractile myofibroblasts. The α-SMA-immunostained sections of the control group demonstrated single layer of α-SMA positive cells around the central vein and weak α-SMA positive cells around the portal vessels (Fig. 7a). The low dose IONP group showed mild immunereactivity around the central vein and increased α-SMA immunereactivity the media of the vessels of the portal area (Fig. 7b). The

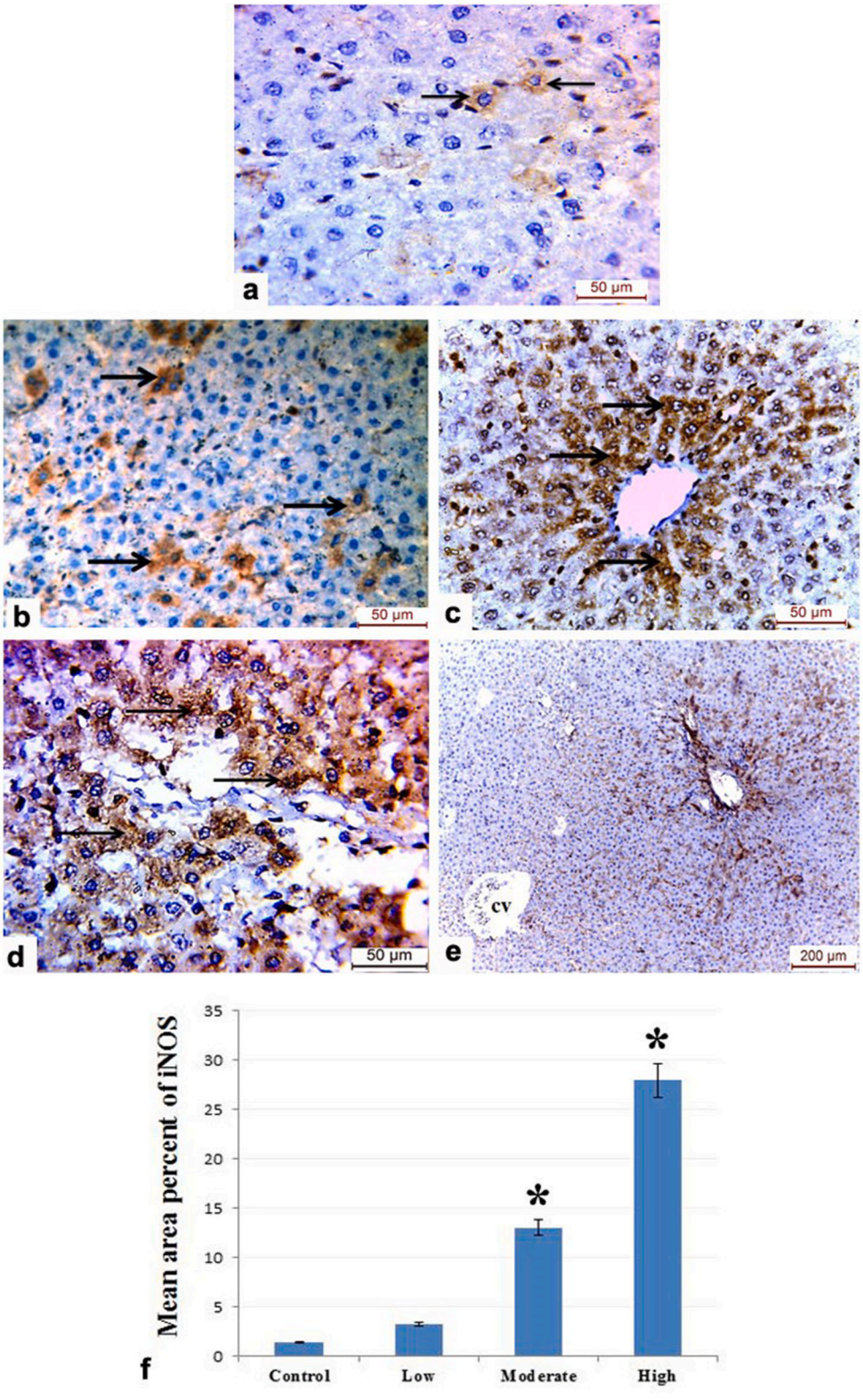


*(caption on next page)*

**Fig. 8.** A photomicrograph of a section in the rat liver from (a) group I (control) showing (a) very mild iNOS expression in the hepatocytes. (b) group II (Low dose) shows mild positive iNOS immunoreactivity. (c) group III (Medium dose) shows strong positive iNOS immunoreactive hepatocytes around the central vein. (d) group IV (High dose) shows intense positive iNOS immunorectivity in the hepatocytes. (arrows pointing to areas of immunoreactivity) (e) group IV (High dose) shows intense positive iNOS reaction in the periportal area with diminution of intensity toward the central vein (cv). (f) Area percentage of iNOS immunreactivity in the different study groups (n = 6); data are presented as mean ± SD. *: Statistically significant compared to corresponding value in: control group at $P < 0.05$ using ANOVA, Bonferroni post-hoc pairwise comparison.

medium dose group displayed strong positive α-SMA immunoreaction in the wall of the central vein and the blood sinusoids and in the media of a dilated portal vein and a thickened hepatic artery (Fig. 7c). The high dose shows intense positive α-SMA immunoexpression around the central vein, in the blood sinusoids between the hepatocytes and in the media of the portal area vessels (Fig. 7d).

The histomorphometric study revealed highly-significant increase in α-SMA immunoexpression of the medium and high dose groups (Fig. 7e). This dose-dependent increase in α-SMA-expression is concomitant with the significant increase in collagen deposition. A possible explanation is that hepatocyte injury leads to generation of lipid peroxides which activates the hepatic stellate cells involved in synthesis of extracellular matrix and α-SMA expression [14].

### 4.5. Immuno-histochemical evaluation of iNOS in the liver tissue

Nitric oxide generated by the inducible form of NOS (iNOS) is implicated with the inflammatory conditions involving monocyte/macrophage lineage cells [15]. This coincides with the results of our study which demonstrated both recruitment of macrophages and up-regulation of iNOS immune-expression in the IONP-treated groups Fig. 8(a–f).

The high dose of IONPs-treated rats demonstrated zonal distribution of iNOS with the strongest expression in the periportal area, with gradual diminution of intensity toward the perivenous regions of the hepatic acinus. This could be attributed to the greatest concentration of IONPs encountered by periportal hepatocytes and/or the previously-reported iNOS zonal gene expression [16].

### 4.6. Effect of IONPs on the renal pathological changes

As a main excretory organ, the kidney is predisposed to several forms of direct/indirect injuries secondary to nanoparticle exposure [17]. In the present work, histological examination of the renal cortex after prolonged administration of IONPs for 28 days has revealed various histopathological and haemodynamic changes Fig. 9(a–e). Among those changes, congestion in the glomerular and peritubular capillaries was an evident feature. These results are due to the interaction of IONPs with the renal biological membranes during passage of IONPs through the filtration barrier [18].

The effect of IONPs on the proximal and distal convoluted tubules in the current study was in the form of cast formation, intraluminal exfoliation of epithelial cells, massive hyaline exudate in the tubular lumen, luminal dilatation and cellular vacuolations. The IONPs-induced tubular damage could be attributed to iron overload which results in massive iron deposition with subsequent necrosis of the proximal tubules [19].

With administration of high dose IONPs, more severe changes such as interstitial hemorrhage and marked mononuclear infiltration were observed. The oxidative stress state produced by INOs exposure is involved in endothelial dysfunction and recruitment of inflammatory cells such as polymorphonuclear neutrophils [20].

The IONPs increased collagen deposition with the high dose group. The ROS products caused by IONPs can cause mitochondrial dysfunction, activating a cascade leading to glomerulosclerosis and tubular-interstitial fibrosis [19].

### 4.7. Evaluation of MT- and PAS staining of the renal tissue

MT-stained sections of the control group showed scanty collagen distribution around the parietal layers of Bowman's capsules and thin basement membrane of the renal tubules. The low dose group demonstrated minimal collagen bundles around the parietal layer of Bowman's capsule, around the glomerular capillary tuft and the basement membrane of the renal tubules. The medium dose group showed moderate increase in collagen fibers around the parietal layer of Bowman's capsule, in the macula densa of the glomerular capillary tuft and in-between the renal tubules and around blood vessels. The high dose group showed marked thickening of basement membranes of the renal tubules and the parietal layer of Bowman's capsule with augmented interstitial collagen fibers around congested blood vessels (Fig. 10).

PAS staining in the current study revealed thickening of the tubular basement membranes and the parietal layers of Bowman's capsules in the high dose IONPs treated-rats Fig. 10(a–j). The glomerular filtration barrier, being the primary site of blood filtration, is crucial in renal function. The excessive free radicals produced by the high dose IONPs accelerate the injury of the filtration membrane and enhance the formation of advanced glycation end-products [21].

### 4.8. Immuno-histochemical evaluation of iNOS and α-SMA in the kidney tissue

The inducible NOS-immune stained sections of the control group showed faint positive iNOS immunoreaction in the renal tubular cells. The low dose showed mild iNOS immunoreactivity in the renal tubular epithelial cells, with negative immunostaining in the glomeruli. The medium dose group displayed moderate iNOS expression in the renal tubular cells. The high dose group showed intense

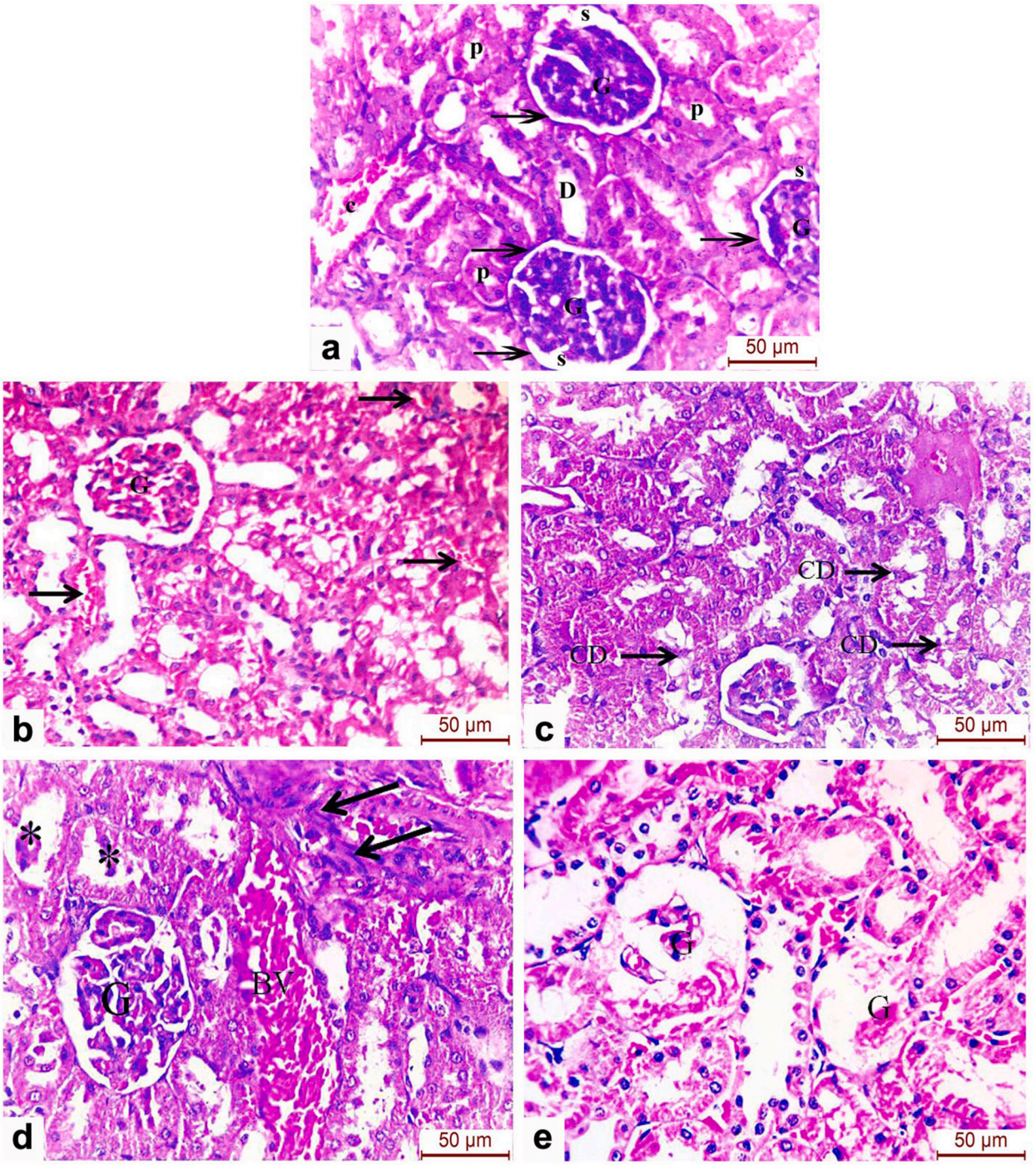


**Fig. 9.** A photomicrograph of a section in the renal cortex from (a) group I (control group) showing (a) glomerulus (G) with its capillary tufts surrounded by the parietal layer of Bowman's capsule (arrows) with a urinary space (S) in between. The proximal convoluted tubules (P) have high cuboidal or columnar epithelial cells and narrow lumina. The lining epithelium of the proximal convoluted tubules has a strong acidophilic cytoplasm and spherical basal nuclei. The distal convoluted tubules (D) show wide lumina, cuboidal lining cells, faint acidophilic cytoplasm and rounded central nuclei. Peritubular capillaries (c) are also noticed. (b) group II (Low dose) shows congested glomerulus (G) and peritubular capillaries (arrows). (c) group III (Medium dose) shows renal tubules with desquamated cellular debris (CD) in their lumina. (d–e) group IV (High dose) shows (d) segmented glomerulus (G) with markedly-congested dilated peritubular blood vessels (BV), thickening of arteriolar wall (arrows) and epithelial casts in the tubular lumina (*). (e) other glomeruli show severe necrosis of the glomerular capillary tuft (G) with marked widening of the urinary space (arrows).

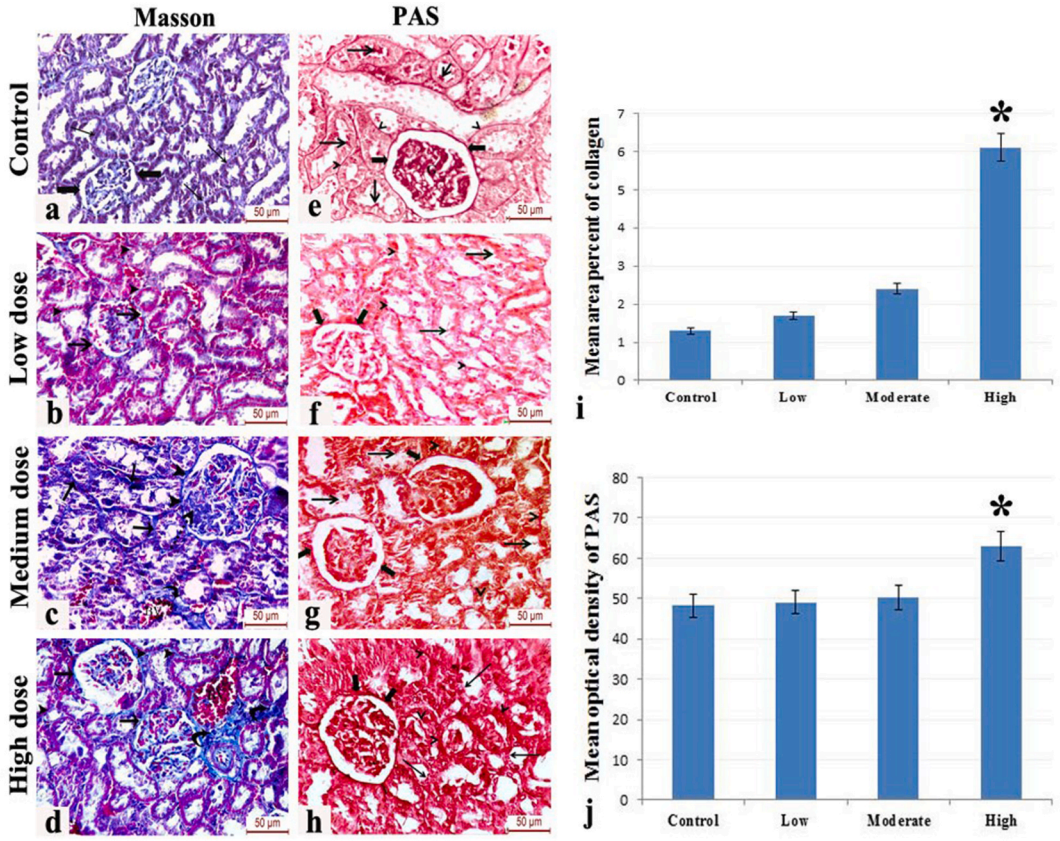


**Fig. 10.** A photomicrograph of a section in the renal cortex showing (a–e) Masson's trichome-stained sections of (a) group I (control group) showing scanty distribution of collagen around the parietal layers of Bowman's capsules (thick arrows) and thin basement membrane of the renal tubules (thin arrows). (b) group II (Low dose) shows minimal collagen bundles around the parietal layer of Bowman's capsule (arrows), around the glomerular capillary tuft (G) and the basement membrane of the renal tubules (arrow heads). (c) group III (Medium dose) shows moderate increase in collagen fibers around the parietal layer of Bowman's capsule (arrow heads), in the macula densa of the glomerular capillary tuft (dotted arrow) and in-between the renal tubules (arrows) and around blood vessels (BV) (curved arrow). (d) group IV (High dose) shows marked thickening of basement membranes of the renal tubules (arrow heads) and the parietal layer of Bowman's capsule (arrows). Augmented interstitial collagen fibers (curved arrow) around congested blood vessels (BV) are also seen. (e–h) PAS-stained sections of (e) group I (control group) normal PAS reaction in the renal glomerulus (G), the apical brush border of convoluted tubules (thin arrows), the parietal layer of Bowman's capsule (thick arrows) and the basement membranes of the renal tubules (arrow heads). (f) group II (low dose) shows mild increase in PAS reaction in the basement membranes of the renal tubules (arrow heads) and the parietal layers of Bowman's capsules (thick arrows). The PAS-stained apical brush borders of the proximal convoluted tubules are intact (thin arrows). (g) group III (Medium dose) showing disrupted PAS reaction of the brush border (thin arrows) of many proximal tubules. Note the moderate PAS reaction of the parietal layers of Bowman's capsules (thick arrows) and the basement membranes of the convoluted tubules (arrow heads). (h) group IV (High dose) showing loss of the apical brush borders of the proximal convoluted tubules (thin arrows). A strong positive reaction of the parietal layer of Bowman's capsule (thick arrows) and the basement membrane of renal tubules (arrow heads) are observed. (i) Area percentage of collagen deposition in the different study groups; (j) Mean optical density of PAS reaction. Data are presented as mean ± SD (n = 6). * tatistically significant compared to corresponding value in: control group at ($P < 0.05$) using ANOVA, Bonferroni post-hoc pairwise comparison.

positive (iNOS) immunostaining reaction Fig. 11 (a-d, i).

Nitric oxide regulates glomerular hemodynamics, release of sympathetic neurotransmitters and tubular functions. The inducible isoform of nitric oxide (iNOS) is known to aggravate renal oxidative damage [22]. Increased iNOS reaction is strongly-linked to inflammation [15] which was proven in the current study by the presence of inflammatory infiltrate.

Alpha-SMA–immuno stained sections of control group showed minimal immunostaining for α-SMA reaction in the renal arterioles. The low dose showed mild expression of α-SMA in the glomerular capillary tuft and peri-tubular capillaries. The medium dose group displayed positive reaction for α-SMA in numerous mesangial cells, in the macula densa and peritubular capillaries. The high dose group displayed strong reaction for α-SMA in the glomerular mesangial cells and in the media of the renal blood vessels Fig. 11 (e-h, j).

Alpha SMA is a fundamental molecular marker for myofibroblasts in various types of nephropathies [23]. The mesangial cells, as well as the renal tubular epithelial cells transform into myofibroblasts under several pathological conditions. These myofibroblasts express α-SMA and produce collagen (type I and type IV) which contribute to development and deterioration of glomerulosclerosis [24]. Increased α-SMA expression has also been previously linked to oxidative stress where the actin fibers were essentially considered

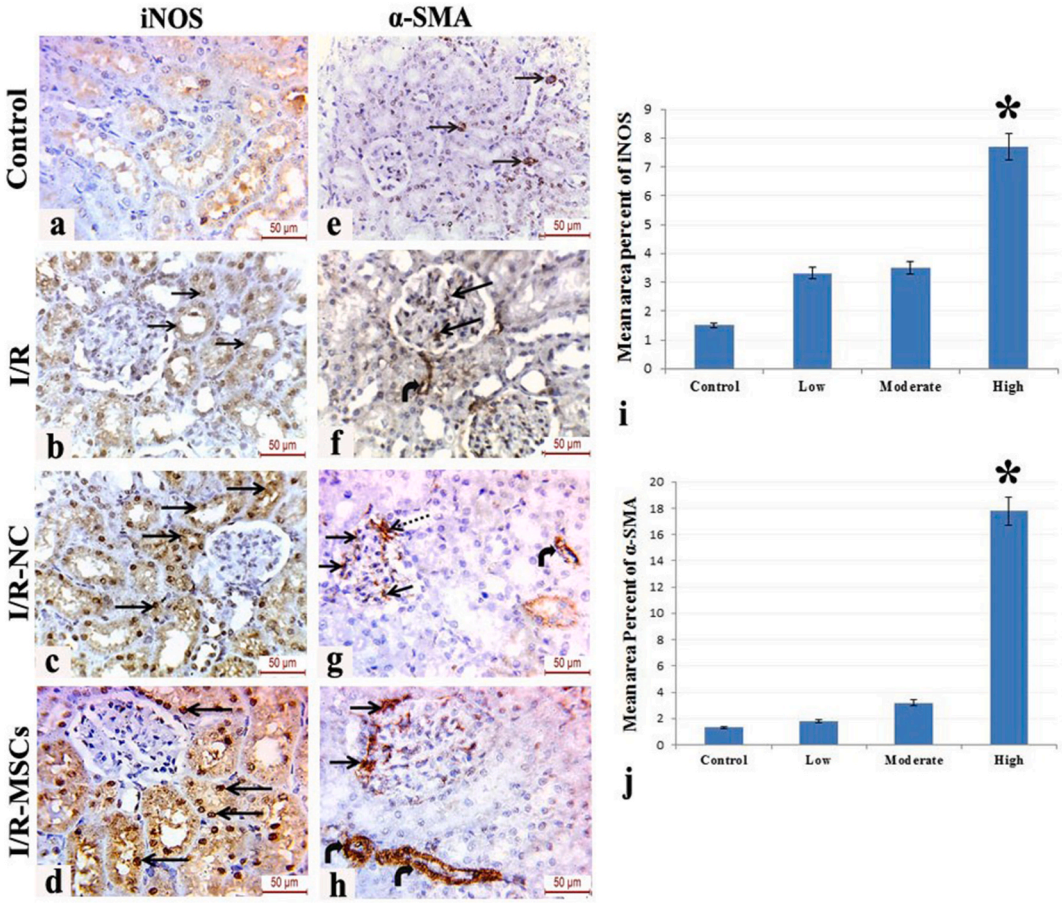


**Fig. 11.** A photomicrograph of a section in the renal cortex showing (a–e) iNOS- immune stained sections of (a) group I (control group) showing faint positive iNOS immunoreaction in the renal tubular cells (arrows). (b) group II (low dose) shows mild iNOS immunoreactivity in the renal tubular epithelial cells (arrows), with negative immunostaining in the glomeruli. (c) group III (Medium dose) showing moderate iNOS immunoreactivity in the renal tubular cells (arrows). (d) group IV (High dose) showing intense positive (iNOS) immunostaining reaction in the renal tubular cells (arrows). (e–h) α-SMA –immuno stained sections of (e) group I (control group) showing minimal immunostaining for α-SMA reaction in the renal arterioles (arrows). (f) group II (Low dose) shows mild expression of α-SMA in the glomerulus capillary tuft (straight arrows) and peri-tubular capillaries (curved arrow). (g) group III (Medium dose) positive reaction for α-SMA in numerous mesangial cells (straight arrows), in the macula densa (dotted arrow) and peritubular capillaries (curved arrow). (h) group IV (High dose) strong reaction for α-SMA in the glomerular mesangial cells (arrows) and in the media of the renal blood vessels (curved arrows). (i) Area percentage of iNOS immunoreactivity in the different study groups. (j) Area percentage of α-SMA immunoreactivity in the different study groups. Data are presented as mean ± SD (n = 6). *: Statistically significant compared to corresponding value in the control group, ($P < 0.05$) using ANOVA, Bonferroni post-hoc pairwise comparison.

as critical stress fibers [25].

### 4.9. Effect of IONPs on kidney and liver functions

To evaluate the effect of the above-mentioned histopathological changes on the hepatic functional performance, the current study evaluated the ALT, AST and ALP as the fundamental parameters reflecting the liver functions (Fig. 12 a,b,c).

The ALT, AST and ALP level in the medium and high dose groups revealed statistically and highly-statistically significant increase, respectively, relative to the control group. Comparison of the different IONPs-treated groups revealed statistically significant difference in ALT level only between high and low dose groups.

Comparison of the different IONPs-treated groups revealed statistically-significant difference in AST and ALP level between the medium and low doses and between the high and low doses.

Hepatic enzymes are the most sensitive biomarkers used for evaluating the functional integrity of liver cells. Thus, elevation of the level of those enzymes is considered a clear evidence for the damage of hepatocytes cell membrane [26] and/or liver necrosis with subsequent leakage of these enzymes into the blood stream [27].

The present work detected a statistically-significant elevation of ALP serum level in all IONPs doses. Elevated ALP level as an indication of damaged reticoloendoplasmic system by the iron nanoparticles [8].

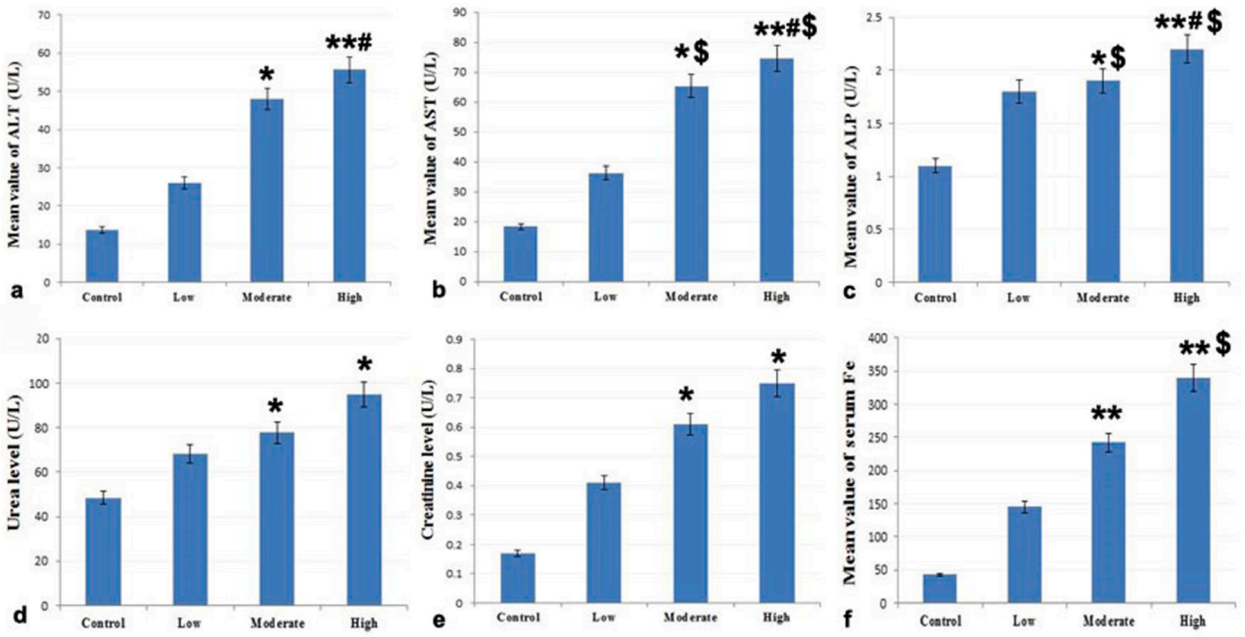


**Fig. 12.** Dose-dependent effect of Iron oxide nanoparticle (IONPs) on the liver and renal functions. (a,b,c) Liver enzymes (a) ALT, (b) AST, (c) ALP levels (U/L). (d,e) Kidney function markers (d) Urea level, (e) Creatinine level and (f) Serum Fe levels, Data are presented as the means ± SD at $p < 0.05$. * significant versus control, ** highly-significant versus control, # significant versus moderate dose group, $ significant versus low dose group.

On the other hand, a previous study [28] reported no elevation of the hepatic enzymes at any time points throughout the 28 days duration of their experiment. A possible explanation could be that the authors used only a single dose of IONPs and this single dose was well-tolerated and did not affect the functional integrity of the liver.

While there was only mild changes in the serum urea and creatinine levels in the low dose group. The moderate and the high dose groups, on the other hand, have revealed a statistically-significant increase in the mean values of those markers (Fig. 12d and e). This suggests that renal function was compromised following administration of IONPs and this compromise was dose dependent.

The augmented urea and creatinine levels in the current study could be related to the oxidative stress state produced by IONPs which lead to lipid peroxidation of biological membrane which in turn leads to change of the membrane potential, increase in permeability, loss of cellular functional integrity and impaired filtration of urea and creatinine [29].

The serum iron levels increased in a dose-dependent manner in the IONP-treated groups. This increase was highly significant in the moderate and high dose groups (Fig. 12f). A previous study has reported a dose-dependent increase of iron level on exposure to different doses of IONPs [30]. The authors also added that histo-pathologic severity was well-corroborated with the increased intensity of iron deposition. The iron ion content of the IONPs is itself a potential cause of toxicity of the iron oxide-based particles [31].

### *4.10. IONPs-induced oxidative stress in the hepatic and renal tissue*

In order to assess the effect of IONPs on the oxidative signaling, the current study has evaluated the levels of three cardinal components of the anti-oxidant system; the SOD, the GPx and the MDA.

There was highly-significant decrease in the SOD activity in all IONPs-treated groups relative to the control group (Fig. 13a). On the other hand, the GPx activity revealed statistically non-significant decrease in the low and medium dose IONPs-treated groups and statistically significant decrease only in the high dose group relative to the control group (Fig. 13b).

Individual antioxidant enzymes play different strategies to counteract oxidative insult. SOD is considered the first line of defense in the antioxidant system. The current study revealed a dose dependent depletion of SOD activity in the liver with IONPs administration. This could be attributed to the heavy influx of superoxide radicals that results in high levels of $H_2O_2$ generation and inhibition of SOD activity.

The statistically-significant decrease in GPx activity in the hepatic tissue of group IV also indicates that the antioxidant defense system is overwhelmed by the amount of ROS leading to consumption of GPx with subsequent oxidative damage of intracellular proteins and DNA. The uptake of nanoparticles by Küpffer cells in the liver could also induce modifications in the hepatocyte anti-oxidant system, such as depletion of GPx or SOD [32].

Assessment of the MDA level in the liver homogenates of the different study groups revealed statistically-significant increase only in the high dose group relative to the control group (Fig. 13c).

The MDA represents the final product of lipid peroxidation, the process in which ROS attacks lipids, especially polyunsaturated fatty acids. The current study illustrated increased MDA level in a dose dependent manner in the liver of IONPs-treated rats.

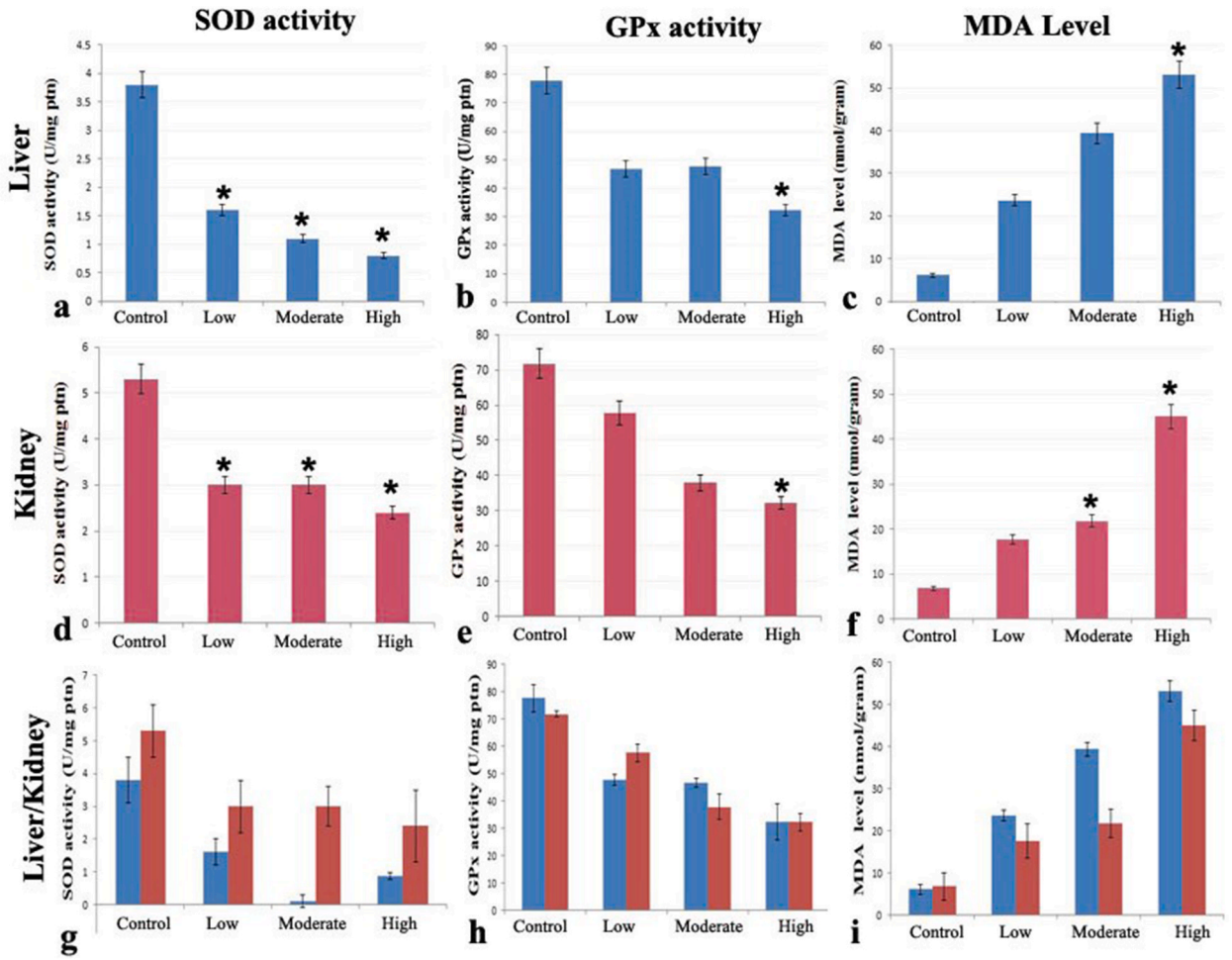


**Fig. 13.** Dose-dependent effect of Iron oxide nanoparticle (IONPs) on the liver and kidney oxidative parameters; (a,d,g) superoxide dismutase (SOD) activity (Unit/mg protein), (b,e,h) glutathione peroxidase (GPx) activity and (c,f,i) malondialdehyde (MDA) level (mmol/mg protein). Data are presented as the means ± SD. * denotes significant change at $p < 0.05$ versus control group.

**Table 1**
Comparison between mean area percentage of masson trichrome and mean optical density of PAS reaction in the liver and kidney of the different groups.

| | | Groups | | |
|---|---|---|---|---|
| | | Liver | Kidney | P-Value |
| **Area % of Masson Trichrome** | **I** | **14.4** ± 2.7 | **1.3** ± 0.6 | 1.000(NS) |
| | II | **22.7** ± 2.5 | **1.7** ± 0.78 | 0.680(NS) |
| | III | **38.4** ± 3.2 | **2.4** ± 1.2 | 0.082(NS) |
| | IV | **54.4** ± 3.9 | **6.1** ± 2.6 | 0.006* |
| | | **Groups** | | |
| | | Liver | Kidney | P-Value |
| **Optical density of PAS reaction** | **I** | **56.4** ± 2.4 | **48.3** ± 1.4 | 1.000 (NS) |
| | II | **53.3** ± 3.6 | **49.1** ± 1.2 | 0.826(NS) |
| | III | **45** ± 3.4 | **50.3** ± 1.8 | 0.021* |
| | IV | **38.9** ± 6 | **63** ± 3 | 0.0003** |

Using ANOVA followed by Bonferroni pairwise comparisons.
*: Statistically significant P value ≤ 0.05.
**: Highly statistically significant P value ≤ 0.001.
NS: Non significant.

**Table 2**
Comparison between mean area percentage of α-SMA and iNOS immunohistochemical reaction in the liver and kidney of the different groups.

| | Groups | Organs | | |
|---|---|---|---|---|
| | | Liver | Kidney | P-Value |
| **Area % of α-SMA** | **I** | **0.98** ± 0.6 | **1.3** ± 0.5 | 1.000 (NS) |
| | II | **2.1** ± 0.21 | **1.8** ± 0.86 | 1.000 (NS) |
| | III | **4.1** ± 0.83 | **3.2** ± 1.4 | 1.000 (NS) |
| | IV | **7.7** ± 1.5 | **17.8** ± 4.3 | 0.0005** |
| | **Groups** | **Organs** | | |
| | | Liver | Kidney | P-Value |
| **Area % of iNOS** | **I** | **1.38** ± 0.7 | **1.5** ± 0.7 | 1.000 (NS) |
| | II | **3.24** ± 1 | **3.3** ± 1.4 | 1.000 (NS) |
| | III | **12.98** ± 2.7 | **3.5** ± 0.5 | 0.0002** |
| | IV | **27.91** ± 1.5 | **7.7** ± 1.6 | 0.0001** |

Using ANOVA followed by Bonferroni pairwise comparisons.
**: Highly statistically significant P value $\leq$ 0.001.
NS: Non significant.

Evaluation of the anti-oxidant parameters in the renal tissue revealed highly-significant decrease in the SOD activity in all IONPs-treated groups relative to the control group (Fig. 13d). Assessment of the GPx activity revealed statistically non-significant decrease in the low and medium dose IONPs-treated groups and statistically significant decrease only in the high dose group (Fig. 13e). Highly-significant increase was observed in the MDA level of the medium and high dose groups relative to the control group (Fig. 13f).

MDA is a typical biomarker for evaluating renal lipid peroxidation injury [33]. The current study illustrated dose-dependent increase of MDA in renal tissue homogenates with increasing the dose of IONPs. This comes in agreement with the previous reports of augmented lipid peroxidation in the kidneys after administration of IONPs for one week [18].

On screening the other oxidative markers, the current study detected decreased GPx and SOD levels in the kidney tissue of the IONPs-treated rats. This decrease, however, was only statistically-significant in the high dose group. The oxidative stress induced by IONPs (evidenced by decreased GPx and SOD activity along with increased MDA level) could be introduced as a postulated mechanism explaining the kidney function impairment and the renal tubular damage [17] owing to the role of IONPs in increasing the ROS level and subsequent exhaustion of the most of the antioxidant enzymes [27].

The SOD and GPx activity as well as the MDA level, revealed non-statistically significant difference between the liver and kidneys (Fig. 13g and h,i).

### *4.11. Comparing the liver versus the kidney parameters*

On comparing the effect of different doses of IONPs between the liver and kidney, the high dose revealed statistically significant difference in area percent of collagen deposition and α-SMA reaction in the liver relative to the kidney. The medium and high doses revealed statistically significant difference in optical density of PAS reaction and area percent of iNOS reaction in the liver relative to the kidney Tables 1 and 2.

## Funding

The authors extend their appreciation to the Ministry of Education in KSA for funding this research work through the project number KKU-IFP2-DC-1.

## Declarations

The study was approved by Kasr Alainy Ethics Committee and the Institutional Animal Care and Use Committee (IACUC) (approval number CU-III F14-19). The study had been conducted according to the ethical standards of the National Institutes of Health guide for the care and use of Laboratory Animals (NIH Publications No. 8023, revised 1978).

## CRediT authorship contribution statement

**Basma Emad Aboulhoda:** Conceived and designed the experiments, Wrote the paper. **Doaa Abdullah Othman:** Conceived and designed the experiments, Performed the experiments, Analyzed and interpreted the data, Wrote the paper. **Laila A. Rashed:** Performed the experiments, Contributed reagents, materials, analysis tools or data. **Mansour A. Alghamdi:** Contributed reagents, materials, analysis tools or data. **Abd EL Wakeel E. Esawy:** Contributed reagents, materials, analysis tools or data.

## Declaration of competing interest

The authors declare that they have no known competing financial interests or personal relationships that could have appeared to influence the work reported in this paper.

## Acknowledgments

The authors extend their appreciation to the Ministry of Education in KSA for funding this research work through the project number KKU-IFP2-DC-1.

## References

[1] L. Wu, W. Wen, X. Wang, D. Huang, J. Cao, X. Qi, S. Shen, Ultrasmall iron oxide nanoparticles cause significant toxicity by specifically inducing acute oxidative stress to multiple organs, Part. Fibre Toxicol. 19 (1) (2022) 1–14.
[2] M.G. Montiel Schneider, M.J. Martín, J. Otarola, E. Vakarelska, V. Simeonov, V. Lassalle, M. Nedyalkova, Biomedical applications of iron oxide nanoparticles: current insights progress and perspectives, Pharmaceutics 14 (1) (2022) 204.
[3] U.S. Ezealigo, B.N. Ezealigo, S.O. Aisida, F.I. Ezema, Iron oxide nanoparticles in biological systems: antibacterial and toxicology perspective, JCIS Open 4 (2021), 100027.
[4] N. Zhang, G. Xiong, Z. Liu, Toxicity of metal-based nanoparticles: challenges in the nano era, Front. Bioeng. Biotechnol. 10 (2022), 1001572.
[5] U.A. Reddy, P.V. Prabhakar, M. Mahboob, Biomarkers of oxidative stress for in vivo assessment of toxicological effects of iron oxide nanoparticles, Saudi J. Biol. Sci. 24 (6) (2017) 1172–1180. .
[6] R.E. Ghoweba, A.A. Khowailed, B.E. Aboulhoda, L.A. Rashed, A. Selmy, Synergistic Role of Resveratrol and Exercise Training in Management of Diabetic Neuropathy and Myopathy via SIRT1/NGF/GAP43 Linkage, Tissue and Cell, 2023, 102014.
[7] M. Hanna, H. Seddiek, B.E. Aboulhoda, G.N. Morcos, A. Akabawy, M.A. Elbaset, A.A. Ibrahim, M.M. Khalifa, I.M. Khalifah, M.S. Fadel, T. Shoukry, Synergistic cardioprotective effects of melatonin and deferoxamine through the improvement of ferritinophagy in doxorubicin-induced acute cardiotoxicity, Front. Physiol. 13 (2022), 1050598.
[8] K. Parivar, F.M. Fard, M. Bayat, S.M. Alavian, M. Motavaf, Evaluation of iron oxide nanoparticles toxicity on liver cells of BALB/c rats, Iran. Red Crescent Med. J. 18 (1) (2016) 28939–28944. .
[9] A. Vasili, G. Sharifi, M. Faramarzi, A. Noori, S. Yazdanshenas, The effect of aerobic exercise on hepatotoxicity induced by intratracheal instillation of iron oxide nanoparticles in Wistar rats, Gen. Physiol. Biophys. 35 (2016) 35–43. .
[10] Y. Yang, Z. Qin, W. Zeng, T. Yang, Y. Cao, C. Mei, Y. Kuang, Toxicity assessment of nanoparticles in various systems and organs, Nanotechnol. Rev. 6 (3) (2017) 279–289. .
[11] G. Martemucci, C. Costagliola, M. Mariano, L. D'andrea, P. Napolitano, A.G. D'Alessandro, Free radical properties, source and targets, antioxidant consumption and health, Oxygen 2 (2) (2022) 48–78.
[12] M. Almansour, S. Alarifi, B. Jarrar, In vivo investigation on the chronic hepatotoxicity induced by intraperitoneal administration of 10-nm silicon dioxide nanoparticles, Int. J. Nanomed. 13 (2018) 2685–2696. .
[13] A.M. Abdel-Hafez, M.A. Othman, Effect of sildenafil citrate on the structure of rat liver: a histological, histochemical and immunohistochemical study, Egyptian Journal of Histology 36 (4) (2013) 991–1003. .
[14] C. Erenoğlu, M. Kanter, B. Aksu, T. Sağıroğlu, S. Ayvaz, C. Aktaş, M. Erboğa, Protective effect of curcumin on liver damage induced by biliary obstruction in rats, Balkan Med. J. 28 (4) (2011) 352–357. .
[15] T.N. Golden, A. Venosa, A.J. Gow, Cell origin and iNOS function are critical to macrophage activation following acute lung injury, Front. Pharmacol. 12 (2022), 761496.
[16] L. McNaughton, L. Puttagunta, M.A. Martinez-Cuesta, N. Kneteman, I. Mayers, R. Moqbel, Q. Hamid, M.W. Radomski, Distribution of nitric oxide synthase in normal and cirrhotic human liver, Proc. Natl. Acad. Sci. USA 99 (26) (2002) 17161–17166. .
[17] Y. Min, G.G.D. Suminda, Y. Heo, M. Kim, M. Ghosh, Y.O. Son, Metal-based nanoparticles and their relevant consequences on cytotoxicity cascade and induced oxidative stress, Antioxidants 12 (3) (2023) 703.
[18] P. Ma, Q. Luo, J. Chen, Y. Gan, J. Du, S. Ding, Z. Xi, X. Yang, Intraperitoneal injection of magnetic Fe3O4-nanoparticle induces hepatic and renal tissue injury via oxidative stress in mice, Int. J. Nanomed. 7 (2012) 4809–4818. .
[19] K. Šebeková, M. Dušinská, K. Simon Klenovics, R. Kollárová, P. Boor, A. Kebis, M. Staruchova, B. Vlkova, B. Celec, J. Hodosy, L. Bačiak, Comprehensive assessment of nephrotoxicity of intravenously administered sodium-oleate-coatedultra-small superparamagnetic iron oxide (USPIO) and titanium dioxide (TiO2) nanoparticles in rats, Nanotoxicology 8 (2) (2014) 142–157. .
[20] S. Gui, Z. Zhang, L. Zheng, Y. Cui, X. Liu, N. Li, X. Sang, Q. Sun, G. Gao, Z. Cheng, J. Cheng, Molecular mechanism of kidney injury of mice caused by exposure to titanium dioxide nanoparticles, J. Hazard Mater. 195 (2011) 365–370. .
[21] B. Martin, N. Caron, I. Jadot, V. Colombaro, G. Federici, C. Depommier, A.É. Declèves, Evaluation of inducible nitric oxide synthase inhibition on kidney function and structure in high-fat diet-induced kidney disease, Exp. Physiol. 103 (1) (2018) 125–140. .
[22] A. Stacchiotti, F. Ricci, R. Rezzani, G.L. Volti, E. Borsani, A. Lavazza, R. Bianchi, L.F. Rodell, Tubular stress proteins and nitric oxide synthase expression in rat kidney exposed to mercuric chloride and melatonin, J. Histochem. Cytochem. 54 (10) (2006) 1149–1157. .
[23] N. Picard, O. Baum, A. Vogetseder, B. Kaissling, M. Le Hir, Origin of renal myofibroblasts in the model of unilateral ureter obstruction in the rat, Histochem. Cell Biol. 130 (1) (2008) 141–155. .
[24] R.G. Fu, T. Zhang, L. Wang, Y. Du, L.N. Jia, J.J. Hou, G.L. Yao, X.D. Liu, L. Zhang, L. Chen, B.S. Gui, Inhibition of the K+ channel KCa3. 1 reduces TGF-β1-induced premature senescence, myofibroblast phenotype transition and proliferation of mesangial cells, PLoS One 9 (1) (2014), e87410.
[25] R. Huang, P. Fu, L. Ma, Kidney fibrosis: from mechanisms to therapeutic medicines, Signal Transduct. Targeted Ther. 8 (1) (2023) 129.
[26] M. Malakouti, A. Kataria, S.K. Ali, S. Schenker, Elevated liver enzymes in asymptomatic patients–what should I do? Journal of Clinical and Translational Hepatology 5 (4) (2017) 394–403. .
[27] M. Kumari, S. Rajak, S.P. Singh, U.S. Murty, M. Mahboob, P. Grover, M.F. Rahman, Biochemical alterations induced by acute oral doses of iron oxide nanoparticles in Wistar rats, Drug Chem. Toxicol. 36 (3) (2013) 296–305. .
[28] S.L. Easo, P.V. Mohanan, Hepatotoxicity evaluation of dextran stabilized iron oxide nanoparticles in Wistar rats, Int. J. Pharm. 509 (1–2) (2016) 28–34. .
[29] N. Singh, G.J. Jenkins, R. Asadi, S.H. Doak, Potential toxicity of superparamagnetic iron oxide nanoparticles (SPION), Nano Rev. 1 (1) (2010) 5358–5363. .
[30] K. Sundarraj, V. Manickam, A. Raghunath, M. Periyasamy, M.P. Viswanathan, E. Perumal, Repeated exposure to iron oxide nanoparticles causes testicular toxicity in mice, Environ. Toxicol. 32 (2) (2017) 594–608. .
[31] B. Pham, E. Colvin, N. Pham, B. Kim, E. Fuller, E. Moon, R. Barbey, S. Yuen, B.H. Rickman, S. Bickley, Biodistribution and clearance of stable superparamagnetic maghemite iron oxide nanoparticles in mice following intraperitoneal administration, Int. J. Mol. Sci. 19 (1) (2018) 205–228. .
[32] Q. Saquib, M. Faisal, A.A. Al-Khedhairy, A.A. Alatar, Cellular and Molecular Toxicology of Nanoparticles, Springer. Orangeburg, NY, USA, 2018, pp. Pp199–213.
[33] C. Mas-Bargues, C. Escriva, M. Dromant, C. Borrás, J. Vina, Lipid peroxidation as measured by chromatographic determination of malondialdehyde. Human plasma reference values in health and disease, Arch. Biochem. Biophys. 709 (2021), 108941.